

Acoustic Emission *RA*-Value and Granite Fracture Modes Under Dynamic and Static Loads



Xiling Liu, Zhou Liu, Xibing Li, and Jiahui Cui

Abstract The *RA*-value characteristics and distribution versus rock acoustic emission average frequency, the peak frequency characteristics, and the evolution of rock fracture modes under dynamic and static loads were studied to understand the fracture modes of rock under dynamic and static loads. The Split-Hopkinson pressure bar system and MTS322 servo-controlled rock mechanical test system were used, respectively, to carry out impact-loading tests and uniaxial compression tests at different loading rates. The results indicate that the *RA*-value under impact loading is higher in the initial stage, decreases to below 1 ms v^{-1} through the failure process, and even the variation trend tends to horizontal lines with loading time, which demonstrates that the fracture modes are dominated by tensile failure. An opposite variation in *RA*-value under static loading results when the loading rate is lower, but the variation corresponds with the impact-loading tests when the loading rate is higher, which indicates that tensile fracture still dominates the failure process and the occurrence of shear failure, as loads peak when the loading rate is lower. The acoustic emission signals exhibit a higher peak frequency under impact loads than those under static loads. Furthermore, in impact-loading tests, the peak *RA*-value will increase gradually with an increase in strain rate. The *RA*-value can be used to classify the crack type and as a rock fragmentation evaluation index. In general, the peak frequency can be used to distinguish two typical signals under impact-loading tests; signals with a higher peak frequency ($f_p > 100 \text{ kHz}$) can be generated by rock fracturing, whereas those with a lower peak frequency and a higher *RA*-value can be generated by elastic wave propagation.

Keywords Rock acoustic emission · *RA*-value · Rock fracture modes · Split-Hopkinson pressure bar · Peak frequency

X. Liu (✉) · Z. Liu · X. Li · J. Cui
Central South University, Changsha, China

1 Introduction

Rocks are mostly polycrystalline and brittle; thus the nucleation and propagation of cracks that are generated by rock failure will emit energy outward as elastic waves when subjected to loading conditions. Such elastic waves that are derived from microscopic dislocations, twinned crystals, crystal interfaces, and the slip and separation of macroscopic mineral grains, joints, and other weak planes are referred to as acoustic emission (AE) activity [1–5]. For polycrystalline and anisotropic rocks, it is a general trend that an extensive understanding of the development and propagation of cracks requires a knowledge of their fracture modes to understand the microscopic failure mechanisms of rocks more easily based on their structural complexity. A very important aspect is the close relationship of the AE parameters to fracture modes (tensile fracture, shear fracture, and their coupling fracture) [6–11]. One of the critical parameters is the *RA*-value, which is a calculated feature that is derived from the “rise time” divided by the “amplitude” in ms v^{-1} and which shows the reciprocal of the gradient in the AE signal waveforms [7, 8]. The *RA*-value is extremely sensitive to the fracture modes. Frequency parameters, such as the average frequency, which is the number of threshold crossings over the signal duration, are measured in kHz. Another important frequency feature is the peak frequency (f_p), which is defined as the point in the power spectrum at which the peak magnitude was observed [11].

Many scholars have presented research on concrete’s fracture modes based on the characteristics of the AE parameters and have shown that the AE signals in shear failure had a longer waveform and lower frequency than those in tensile failure [9, 10]. Shear failure dominated at the last failure stages, whereas initially, the tensile mode was mostly active [12–14]. Several studies have shown that shear cracks lead to AE signals with a higher *RA*-value and lower frequency characteristics than tensile cracks [8, 15]. However, a series of achievements has been made specifically for rocks. For example, Shiotani [7] considered that the variation gradient of the ascending part in the waveform increased, which indicates that cracks of the tensile type were generated predominantly, whereas smaller values correspond to those that occur by shear type. Yang [16] proved that shear failure was a major microscopic failure mechanism of rock in a triaxial compression test that is based on a moment tensor analysis. Cheon [17] proposed that the current damage level of the rock slope and fracture type can be evaluated by changing trends and variation ranges of the AE parameters. Bucheim [18] pointed out that the AE signals of rock samples were characterized by a long duration time and a wide frequency spectrum when subjected to shear failure, whereas the results contrasted in tensile failure. Wang [19] demonstrated that AE signals always exhibited a higher amplitude and lower frequency in shear mode compared with a lower amplitude and higher frequency in tensile mode in three-point bending and shear fracture tests.

In previous work, tensile and shear failure phenomenon were distinguished by their AE behaviors. Limited related work exists on the failure mechanism and AE characteristics of rock under impact loads. Therefore, we investigated the *RA*-value

characteristics and its distribution versus the average frequency of the rock AE, the peak frequency characteristics, and the evolution of rock fracture modes under dynamic and static loading tests.

2 Experimental Details

2.1 Sample Preparation

To compare the fracture modes of rock under different loading conditions, an igneous rock granite was selected for impact and uniaxial compression loading tests. Five rock samples were prepared for each loading test, and their basic data are listed in Table 1.

2.2 Experimental Setup

Many comparisons between dynamic and static rock properties exist in rock mechanics and rock engineering [20]. Because the loading rate matches the drilling and blasting, a 50-mm-diameter Split-Hopkinson pressure bar (SHPB), as recommended by the International Society for Rock Mechanics Commission on Rock Dynamics, was used for the impact-loading test as shown in Fig. 1. A PCI-2 system and one ultra-mini sensor-PICO with a 550-kHz resonant frequency were used to collect the AE signals. The AE signals as detected by the sensor were pre-amplified by 40 dB. The detection threshold and sampling rate were set at 45 dB and 40 Msps, respectively. A MTS322 servo-controlled rock mechanical test system was used to carry out the uniaxial compression tests. In the uniaxial compression tests, the displacement control mode was used, with a loading speed of

Table 1 Basic data statistics of each specimen

Loading conditions	Sample code	Diameter (mm)	Height (mm)	Density (g cm^{-3})	Wave velocity (m s^{-1})
Impact-loading tests	A1	47.92	26.06	2.64	4137.21
	A2	47.83	25.91	2.64	4178.67
	A3	47.72	26.11	2.67	4280.19
	A4	47.81	26.25	2.63	4303.15
	A5	47.85	25.70	2.59	4355.81
Uniaxial compression tests	B1	48.02	98.41	2.62	4432.88
	B2	47.78	99.06	2.65	4762.50
	B3	47.78	99.06	2.65	4762.50
	B4	47.79	97.56	2.66	4414.48
	B5	47.74	96.85	2.65	4656.25

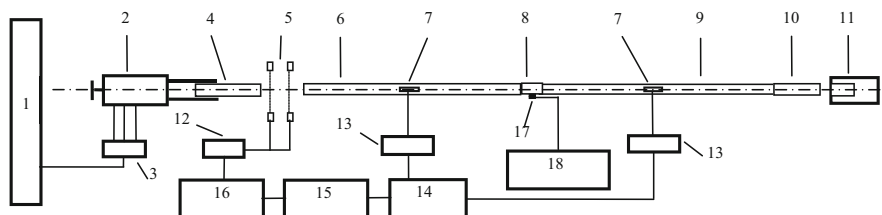


Fig. 1 Schematic of Split-Hopkinson pressure bar system with acoustic emission (AE) testing device. (1) Gas tank, (2) pressure vessel, (3) control valve, (4) striker, (5) light beams, (6) input bar, (7) strain gauge, (8) specimen, (9) output bar, (10) absorption bar, (11) dash pot, (12) electronic counter, (13) bridge, (14) ultra-dynamic strain gauge, (15) transient wave memory, (16) data processing unit, (17) AE sensor, (18) AE signal collecting and processing unit

0.0025, 0.025, and 0.25 mm s⁻¹, respectively. A PCI-2 system and the ultra-mini sensor-PICO with a 550-kHz resonant frequency were used for AE signal collecting. Four sensors were arranged on the cylindrical surface for measurements during uniaxial compression testing. AE signals that were detected by the sensor were pre-amplified by 40 dB. The detection threshold and sampling rate were set to 40 dB and 10 Msps, respectively.

3 Experimental Results and Discussion

3.1 Analysis of RA-Value and Frequency Characteristics

The distribution of *RA*-value versus time from the static- and impact-loading tests (Fig. 2) shows that the *RA*-value under impact loading is higher in the initial stage and decreases suddenly to less than 1 ms v⁻¹ through all fracture levels, and the variation trend tends to a horizontal line with the fracture progress. During the static loading tests, the *RA*-value is less than 20 ms v⁻¹ in the early stage and then exceeds 100 ms v⁻¹ during the fracture strength at a lower loading rate. With an increase in loading rate, the signals with a higher *RA*-value approach those of the initial stage, namely, the variation of *RA*-value, agree with the impact loading. The reasons can be derived from the impact of the equipment on the rock samples, which expands horizontally before the crack initiation, and leads to an increase in amplitude and rise time of the AE signals. However, the increase in rise time exceeds the amplitude significantly. The above results indicate that the granite fracture mode changes from a shear- to a tensile-type fracture with the progress of the fracture, but the fracture modes are dominated by tensile failure under impact loading. In static loading tests, the opposite occurs when the loading rate is lower; whereas the result agrees with the impact loading, when the loading rate is higher. These results prove that the granite fracture modes are more inclined to tensile failure with an increase in loading rate.

Unfortunately, the major fracture mode cannot be obtained under static loading in Fig. 2. Much research [9–12, 21] has shown that the *RA* and average frequency (*AF*)

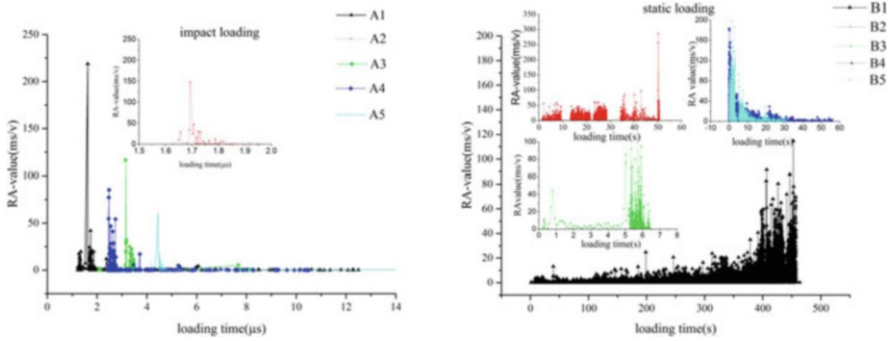


Fig. 2 Variation of *RA*-value with loading time under impact loading (left) and static loading (right) in granite. Numbers A1–A5 represent different strain rates of 115, 109, 103, 85, and 72 s⁻¹, respectively, under impact loading. Numbers B1–B5 represent different loading rates of 0.0025, 0.025, 0.25, 2.5, and 25 mm s⁻¹, respectively, under static loading

distribution of each sample could evaluate the type of fracture. AE signals that are emitted from rock have a higher *RA*-value and a lower average frequency in shear failure than those in tensile failure. Figure 3 shows the *RA* and *AF* distribution of each sample (B1–B5) under uniaxial compression tests. Because much less data were collected for sample B3, the *RA* and *AF* distribution analyses for sample B3 were not performed. The left figure shows the distribution of the original *RA* and *AF* values, whereas the right figure shows the data density map as processed in MATLAB, which is better for visualizing the distribution features. The red squares cover the high-density core data, and they tend to approach the vertical axis, which indicates that in the uniaxial compression test, the granite fracture mode is dominated by tensile failure. This result agrees well with the common understanding that 90% of fractures in rock material under uniaxial compression loads results from tensile failure [22].

From the above results, we conclude that the rock fracture modes are dominated by tensile failure under dynamic and static loads. The evolution of rock fracture modes varies for these two loading conditions. The fracture morphology also proves this point, as shown in Fig. 4. The macroscopic crack propagation direction deviates from the axial pressure direction at a lower loading rate. As the loading rate increases, the direction of macro-crack propagation is parallel to the axial pressure, that is, the macroscopic fracture morphology of granite changes gradually from shear to tensile failure. At a higher loading rate, the macroscopic fracture morphology is the same as that which occurs under impact loading, namely, axial cracks are formed.

The abovementioned AE descriptor (*RA*-value) is one of the most powerful in discriminating fracture modes [17, 18]. However, the individual fracture modes result in differences in other AE parameters, such as amplitude and peak frequency (*f_p*). Figure 5 shows the average peak frequencies and amplitudes for the two loading tests. The AE signals exhibit a higher amplitude and peak frequency under impact-loading tests than those under uniaxial compression tests. In general, it

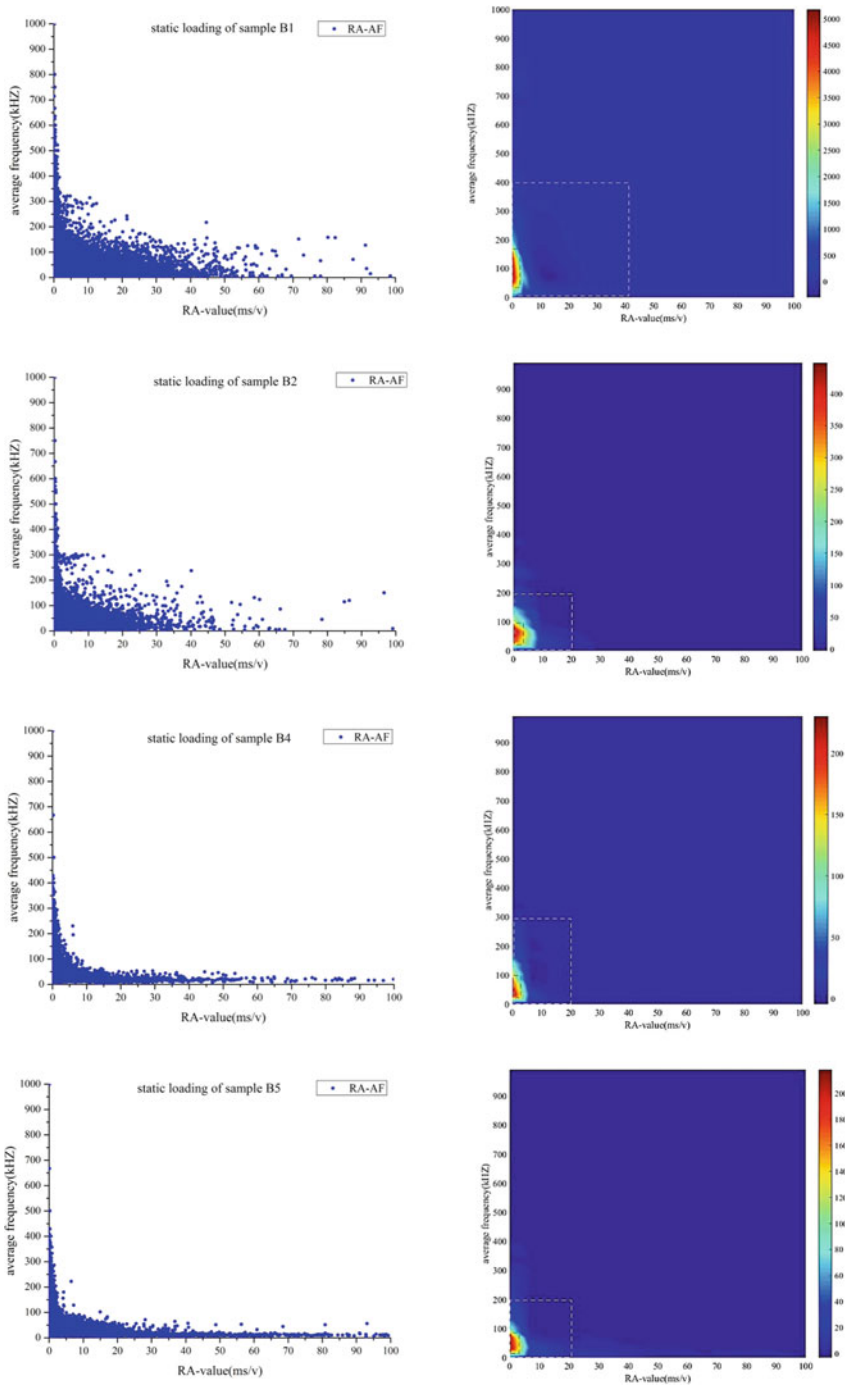


Fig. 3 AF versus *RA*-value for uniaxial compression test of granite. Numbers B1–B5 represent different loading rates of 0.0025, 0.025, 0.25, 2.5, and 25 mm s⁻¹, respectively, under static loading

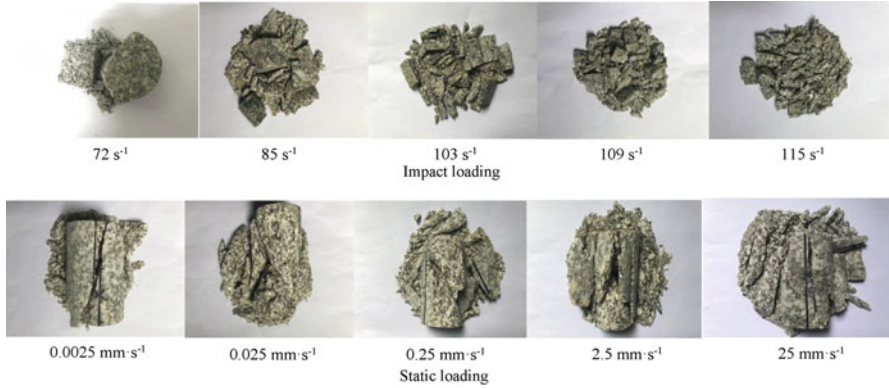
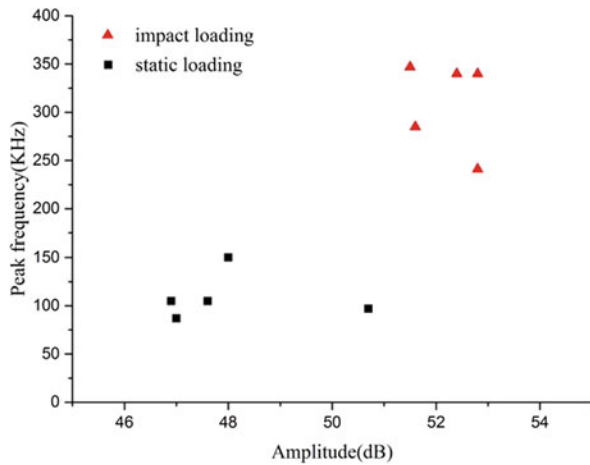


Fig. 4 Fracture morphology for static loading and impact-loading tests of granite

Fig. 5 Peak frequency versus amplitude for different loading conditions (each symbol is the average of all AE events in each experiment)



is accepted that AE signals exhibit a higher frequency in tensile mode compared with a lower frequency in shear mode [9–12, 19]. Although the granite fracture modes are dominated by tensile failure under static loading, the above results prove the existence of shear failure under static loads, which leads to the entire peak frequency (f_p) in the uniaxial compression tests being smaller than in the impact-loading tests.

3.2 Analysis of Waveforms in Impact-Loading Tests

In the impact experiment, the sensor on the rock sample will receive a signal that is generated by elastic stress-wave propagation, which can be considered an inherent characteristic of the rock AE under an impact load. However, if we distinguish the signal from the elastic wave propagation and that generated by rock fracturing, it

should be helpful to understand the fracture characteristics of rock under the impact-loading conditions. In the AE signal parameters, frequency is a major parameter that represents the source characteristics of the elastic waves. According to the stress-wave signals that are detected by the sensor that is glued on the elastic bar in this experiment, the peak frequencies of these stress-wave signals are less than 100 kHz, and the signals that are generated by the stress waves in the rock specimen should be similar in waveform to those recorded by the input elastic pressure bar of the SHPB system. Therefore, we divide the AE signals of rock under an impact load into two parts, namely, those that exceed 100 kHz and those below 100 kHz at peak frequency. Table 2 lists the corresponding *RA*-value for these two signals and shows that the *RA*-value of the signal below 100 kHz at a peak frequency varies significantly, whereas those of the signals that exceed 100 kHz at a peak frequency change only slightly. It can be inferred that signals that exceed 100 kHz derive mainly from rock fracturing, but additional analytical methods are required to verify this result, such as the correlation analysis of signals.

The coefficient of correlation can be used as an indicator to evaluate the similarity of signals in digital signal processing. If $x(n)$ and $y(n)$ are two AE signals, then the coefficient of correlation can be defined as follows:

$$\rho_{xy} = \frac{\sum_{n=1}^L x(n)y(n)}{[\sum_{n=1}^L x^2(n) \sum_{n=1}^L y^2(n)]^{1/2}}$$

where L is the length of the signals. The formula above shows that $|\rho_{xy}| \leq 1$. If two signals are correlated completely (the same signal), then $|\rho_{xy}| = 1$. If two signals are independent, $\rho_{xy} = 0$. The strength of the correlation also depends on a significant-difference *t*-test.

Figure 6 shows the waveform of a typical signal that is recorded on an input elastic bar. Figures 7 and 8 show the waveforms of typical signals that are recorded on rock samples with a peak frequency (f_p) that is lower and higher than 100 kHz, respectively. The waveform in Fig. 7 is more similar than that in Fig. 6. The calculated correlation coefficients of the various typical waveforms in Table 3 also show their similarity.

In Table 3, symbol E is used to represent the waveform that is collected on the input bar. Symbols H1 and H2 are used to represent the waveforms of the signals with a higher peak frequency. Symbols L1 and L2 are used to represent the waveforms of signals with a lower peak frequency and a higher *RA*-value. The results show that signals H1 and H2 exhibit no correlation with that of E because $p > 0.05$. These results indicate that signals with a higher peak frequency are generated by rock failure, whereas the comparison between the signals of L1, L2, and E is statistically significant because $p < 0.05$. Although the ρ_{xy} of L1 and L2 is less than 1, it is larger than that of H1 and H2, so the signals of L1 and L2 could be derived from the elastic pressure bar, combined with the similarity of the waveform

Table 2 RA-value for peak frequencies (f_p) below and above 100 kHz for each specimen impact-loading test

Sample code	A1		A2		A3		A4		A5	
Peak frequency (f_p) (kHz)	$f_p < 100$	$f_p > 100$	$f_p < 100$	$f_p > 100$	$f_p < 100$	$f_p > 100$	$f_p < 100$	$f_p > 100$	$f_p < 100$	$f_p > 100$
RA-value (ms v^{-1})	0-219	0-14	0-150	0-8	0-120	0-6	0-85	0-10	0-61	0-8

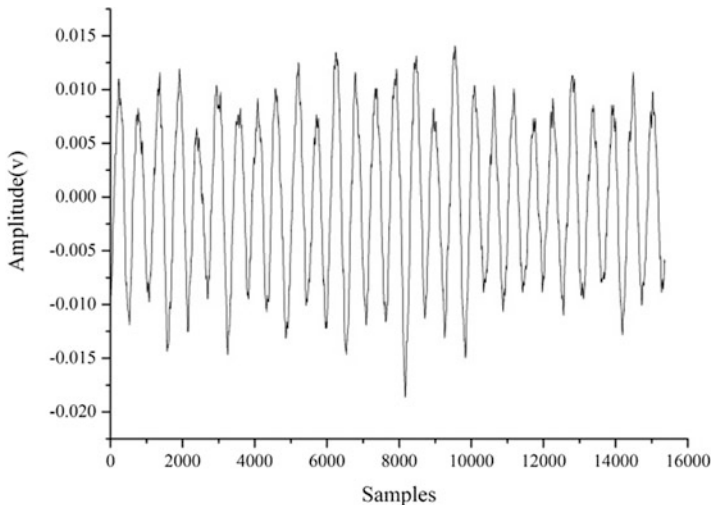


Fig. 6 Typical waveform of a hit that is recorded on the elastic pressure bar

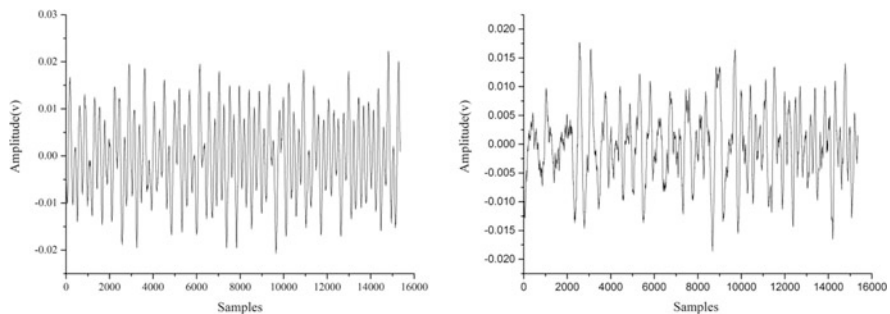


Fig. 7 Two typical waveforms of a hit from a rock sample with a peak frequency below 100 kHz and an RA -value that exceeds 20 ms v^{-1}

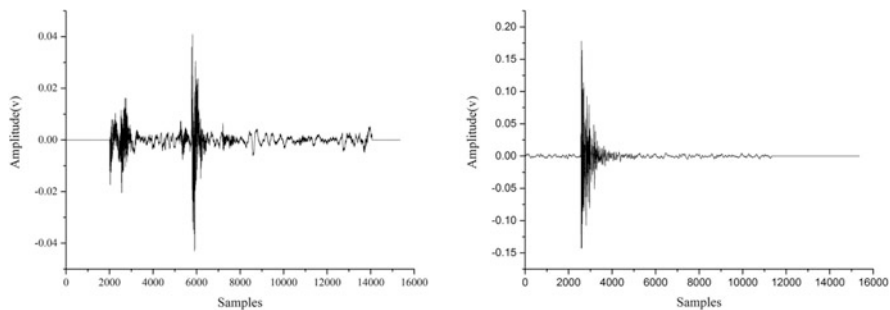


Fig. 8 Two typical waveforms of a hit from a rock sample with a peak frequency that exceeds 100 kHz

Table 3 Calculated correlation coefficient of above waveform

Symbol	Parameter	E	H1	H2	L1	L2
E	Pearson ρ_{xy}	1	0.000	0.004	-0.018*	0.061**
	<i>t</i> -test p (two-tailed)		1.000	0.604	0.023	0.000
H1	Pearson ρ_{xy}	0.000	1	-0.153**	-0.006	-0.001
	<i>t</i> -test p (two-tailed)	1.000		0.000	0.486	0.914
H2	Pearson ρ_{xy}	0.004	-0.153**	1	-0.062**	-0.091**
	<i>t</i> -test p (two-tailed)	0.604	0.000		0.000	0.000
L1	Pearson ρ_{xy}	-0.018*	0.006	-0.062**	1	-0.051**
	<i>t</i> -test p (two-tailed)	0.023	0.486	0.000		0.000
L2	Pearson ρ_{xy}	0.061**	-0.001	-0.091**	-0.051**	1
	<i>t</i> -test p (two-tailed)	0.000	0.914	0.000	0.000	

Remarks: *, significant correlation on 0.05 level (two-tailed); **, significant correlation on 0.01 level (two-tailed)

features. To analyze their correlation, a *t*-test was used as an evaluation index to distinguish the signals of the elastic wave propagation from the signals that are generated by rock fracture based on the existence of elastic waves under impact-loading tests. From the above results, we can probably conclude that signals with a higher peak frequency ($f_p > 100$ kHz) can be thought of as AE signals that are generated by rock fracturing. Those with a lower peak frequency and higher RA-value can be regarded as signals of elastic wave propagation. Therefore, if the signals of the elastic wave propagation are eliminated, the RA-value will be below 1 ms v^{-1} through the failure process. Even the variation trend tends to horizontal lines with loading time, as shown in Fig. 2, which indicates that tensile failure dominates the fracturing process when rock is subjected to impact loads.

4 Conclusions

Under dynamic and static loads, the granite fracture modes are dominated by tensile failure. The evolution of granite fracture modes varies with different loading conditions: the granite fracture modes convert from tensile failure to shear failure under uniaxial compression tests when the loading rate is lower, whereas tensile failure tends to dominate the failure process. The RA-value under static loading is higher in the later period at a lower loading rate, which indicates the occurrence of shear failure as loads peak. If the signals of elastic wave propagation are eliminated, the RA-value will be lower at even less than 1 ms v^{-1} , and the variation trend tends to horizontal lines throughout the fracture process, which indicates that tensile failure dominates the fracturing process when granite is subjected to impact loads.

The AE signals always exhibit a higher peak frequency ($f_p = 250\text{--}400$ kHz) under impact-loading tests compared with those under uniaxial compression tests. Although $f_p = 100$ kHz cannot be used as a boundary to distinguish signals that are

generated by elastic stress-wave propagation from those generated by rock fracturing, the peak frequency can be used to distinguish two typical signals under impact-loading tests. The signals with a higher peak frequency ($f_p > 100$ kHz) can be generated by rock fracturing, whereas those with a lower peak frequency and a higher RA -value can be generated by elastic wave propagation.

Acknowledgments This work is supported by the National Key Research and Development Plan (Project No. 2016YFC0600706), the National Natural Science Foundation of Human Province, China (Grant No. 2016JJ3148), and the Open-End Fund for the Valuable and Precision Instruments of Central South University (CSUZC201701). The authors are extremely grateful for the financial support provided by these funds.

References

1. K. Mogi, Study of the elastic shocks caused by the fracture of heterogeneous materials and its relation to earthquake phenomena. *Bull. Earthq. Res. Inst.* **40**, 125–173 (1962)
2. C.H. Scholz, The frequency-magnitude relation of microfracturing in rock and its relation to earthquakes. *Bull. Seismol. Soc. Am.* **58**, 399–415 (1968)
3. C.H. Scholz, Experimental study of the fracturing process in brittle rock. *J. Geophys. Res. Atmos.* **73**, 1447–1454 (1968)
4. C.H. Scholz, Microfracturing and inelastic deformation of rock in compression. *J. Geophys. Res.* **73**, 1417–1432 (1968)
5. X.L. Liu, X.B. Li, Acoustic emission characteristics of rock under impact loading. *J. Cent. South Univ.* **22**(9), 3571–3577 (2015)
6. S. Yuyama, Z.W. Li, Y. Ito, et al., Quantitative analysis of fracture process in RC column foundation by moment tensor analysis of acoustic emission. *Constr. Build. Mater.* **13**(1–2), 87–97 (1999)
7. T. Shiotani, M. Ohtsu, K. Ikeda, Detection and evaluation of AE waves due to rock deformation. *Constr. Build. Mater.* **15**(5–6), 235–246 (2001)
8. D. Soulioti, N.M. Barkoula, A. Paipetis, et al., Acoustic emission behavior of steel fibre reinforced concrete under bending. *Constr. Build. Mater.* **23**(12), 3532–3536 (2009)
9. D.G. Aggelis, A.C. Mpalaskas, T.E. Matikas, Investigation of different fracture modes in cement-based materials by acoustic emission. *Cem. Concr. Res.* **48**(2), 1–8 (2013)
10. D.G. Aggelis, A.C. Mpalaskas, D. Ntalakas, et al., Effect of wave distortion on acoustic emission characterization of cementitious materials. *Constr. Build. Mater.* **35**, 183–190 (2012)
11. D.G. Aggelis, T.E. Matikas, Effect of plate wave dispersion on the acoustic emission parameters in metals. *Comput. Struct.* **98–99**(5), 17–22 (2012)
12. D.G. Aggelis, Classification of cracking mode in concrete by acoustic emission parameters. *Mech. Res. Commun.* **38**(3), 153–157 (2011)
13. C.U. Grosse, F. Finck, Quantitative evaluation of fracture processes in concrete using signal-based acoustic emission techniques. *Cem. Concr. Compos.* **28**(4), 330–336 (2006)
14. K. Ohno, M. Ohtsu, Crack classification in concrete based on acoustic emission. *Constr. Build. Mater.* **24**(12), 2339–2346 (2010)
15. Y. Lu, Z. Li, W.I. Liao, Damage monitoring of reinforced concrete frames under seismic loading using cement-based piezoelectric sensor. *Mater. Struct.* **44**(7), 1273–1285 (2011)
16. S.Q. Yang, H.W. Jing, S.Y. Wang, Experimental investigation on the strength, deformability, failure behavior and acoustic emission locations of red sandstone under triaxial compression. *Rock Mech. Rock Eng.* **45**(4), 583–606 (2012)

17. D.S. Cheon, Y.B. Jung, E.S. Park, et al., Evaluation of damage level for rock slopes using acoustic emission technique with waveguides. *Eng. Geol.* **121**(1), 75–88 (2011)
18. W.W. Bucheim, *Geophysical Methods for the Study of Rock Pressure in Coal and Potash Salt Mining* (International Strata Control Congress, Leipzig, 1958), p. 222
19. H.J. Wang, D.A. Liu, Z.D. Cui, et al., Investigation of the fracture modes of red sandstone using XFEM and acoustic emissions. *Theor. Appl. Fract. Mech.* **85**, 283–293 (2016)
20. K.W. Xia, W. Yao, Dynamic rock tests using split Hopkinson (Kolsky) bar system – a review. *J. Rock Mech. Geotech. Eng.* **7**(1), 27–59 (2015)
21. S. Rippengill, K. Worden, K.M. Holford, et al., Automatic classification of acoustic emission patterns. *Strain* **39**(1), 31–41 (2010)
22. G. Manthei, Characterization of acoustic emission sources in a rock salt specimen under triaxial load. *Bull. Seismol. Soc. Am.* **95**(5), 1674–1700 (2004)